

An Approximate Thermo-Mechanical Solution of a Functionally Graded Cylinder Using Hybrid Integral Transform and Finite Element Method

M. Dehghan, A. Moosaie^{*}, M. Zamani Nejad

Department of Mechanical Engineering, Yasouj University, Yasouj, Iran

Received 2 September 2021; accepted 19 November 2021

ABSTRACT

This article introduces a novel mixed method that combines the Fast Fourier Transform technique and a conventional Finite Element Method for investigating thermo-mechanical behavior of a thick functionally graded cylinder under asymmetric loadings. Material properties are assumed to vary along the radial direction according to a power function. Thermo-elastic governing equations of the cylinder are derived using principle of virtual work in cylindrical coordinates. Plane strain assumption is considered for a long cylinder during the analysis. Fast Fourier Transform technique is utilized in circumferential direction to discretize equations and related boundary conditions. Finite element method is then applied to remaining equations. For convergence study, the results obtained from this method are compared with those extracted from exact and complete FE solutions. It is observed from the results that the method has a super algebraic convergence behavior in circumferential direction. Influence of the mesh refinement is also investigated in the radial direction. According to ability of the mixed FFT-FE method for asymmetric analyzing, two kinds of loadings are considered here and results are presented. In thermo-elastic analyzing of the long cylinder, it's obvious that the present method benefits from some features such as fast convergence and low computational cost in comparison with FE solution.

© 2022 IAU, Arak Branch. All rights reserved.

Keywords: Thick functionally graded cylinder; Thermo-elastic analysis; Asymmetric loading; Hybrid FFT-FE method.

1 INTRODUCTION

THIN and thick shells of revolution as structural elements cover many branches of technologies such as mechanical, aeronautical, and marine engineering. For example, it can be referred to large span roofs, cooling towers, liquid-retaining structures, water tanks and concrete arch domes in civil and architectural engineering. Shell structures in mechanical engineering are widely used in piping systems, turbines, aircrafts, missiles, rockets, ships and pressure hull of submarines. These structures can efficiently support applied external forces due to their

^{*}Corresponding author. Tel.: +98 74 31005000; Fax.: +98 74 31005000.
E-mail address: moosaie@yu.ac.ir (A. Moosaie)

geometrical shape. In other words, shells are much stronger and stiffer than other structural shapes. Functionally Graded Materials (FGM) are inhomogeneous composite materials which are consisted of a blend of two (or more) materials. The composition of these materials is considered such that the physical (mechanical, thermal, etc.) properties vary smoothly and continuously in desired spatial direction(s). The thermal effects on these structures caused by different phenomena can have serious consequences for their strength and stability. There are many studies in the literature in which the functionally graded cylinders have been investigated with various solution methods. Obata and Noda [1] investigated the steady thermal stresses in a hollow circular cylinder and a hollow sphere made of a functionally gradient material. Jabbari et al. [2] analyzed steady-state thermal stresses in a hollow thick cylinder made of functionally graded material under axi-symmetric and asymmetric loading [3]. The analytical solution of transient thermo-elastic problem involving a functionally graded hollow cylinder due to uniform heat supply is obtained by Ootao and Tanigawa [4]. The transient thermo-elastic analysis of functionally graded cylindrical shells under moving boundary pressure and heat flux by using mixed FE-DQ method has been done by Malekzadeh and Heydarpour [5]. The perturbation technique was employed by Moosaie [6-8] to solve the nonlinear heat conduction and thermo-elastic problems of a thick-walled cylinder made of functionally graded material. Zamani Nejad and his co-workers [9, 10] could derive the governing equations of functionally graded shells of revolution in general curvilinear coordinate system. They also used the Higher-order Shear Deformation Theory (HSDT) and Multi-Layer Method (MLM) for thermo-elastic analysis of Functionally Graded (FG) rotating thick cylindrical and conical shells with variable thickness [11]. In both plane stress and plane strain conditions, stress analysis of the functionally graded rotating thick cylindrical pressure vessels is performed based on the Frobenius series method by Gharibi et al. [12]. Due to the advantages of functionally graded piezoelectric materials (FGPM), some critical issues and problems in the development of thick shells made from these class of materials are discussed by Zamani Nejad et al. [13]. For the case of simplicity in shells of revolution, Fourier transform can be suitably used in circumferential direction. Fast Fourier Transform (FFT) gives numerous advantages such as computer implementation and fast convergence for solving this type of problems. Numerical methods may be inherently accompanied with some deficiencies in modeling of geometry; discretization and satisfaction of boundary conditions. Semi-analytical and mixed methods seem to be appropriate ways to overcome these shortcomings. In this article, FFT technique and FE method are combined to achieve more advantages in analysis of shells of revolution. Proposed mixed method reduces the two-dimensional equilibrium equations to 1-D and is an extreme time saver in thermo-elastic analysis of functionally graded cylindrical shell subjected to asymmetric loads. In this method Discrete Fourier Transform is used to project the equations in Fourier space. Inverse Discrete Fourier Transform is then used to project back to physical space. This computational strategy reduces the cost of thermo-elastic analysis of shells of revolution. Formulation derivation in current work is based on two-dimensional theory of elasticity with plane strain assumptions. To date, some mixed methods are introduced by combination of mathematical techniques like conventional FEM and DQ for free vibration analyzing of thick plates resting on elastic foundation [14]. The time-dependency in a nonlinear thermal problem was removed [15] by effective combination of the Laplace transform and finite element method. A novel computational procedure based on finite differences method and league championship algorithm was provided to solve a one-dimensional inverse heat conduction problem by Ebrahimi et al. [16]. Ozkan and Mengi [17] proposed a new numerical method for the boundary element analysis of axisymmetric bodies. The method was based on complex Fourier series expansion of boundary quantities in circumferential direction, which reduces the boundary element equation to an integral equation. Recently, an efficient combination of Laplace transform and multi-scale finite-element method was presented for coupling partial differential equations of flow in a dual-permeability system by Liu et al [18]. The most commonly used approach for the analysis of shells of revolution is based on the representation of the shell variables and loads by a Fourier series in the circumferential coordinate, combined with the use of a numerical discretization technique (such as finite elements, finite differences or numerical integration) in the meridional direction. For example, this capability was performed for stress and free vibration analyses of laminated anisotropic shells of revolution by Noor and Peters [19]. At first, the coupling effect between symmetric and anti-symmetric modes for composite laminated shells of revolution was investigated by using the mentioned semi-analytical method [20]. Sivadas and Ganesan [21] studied effect of coupling due to the symmetric and antisymmetric modes on vibration characteristics on moderately thick composite laminated shells of revolution using double Fourier series approximation and Finite Element method. The latter semi-analytical method was then widely used by Santos and his coworkers [22-26] for 3-D analysis of axisymmetric shells of revolution with and without piezoelectric sensors and actuators. Special emphasis in these articles was given to the coupling between symmetric and anti-symmetric terms in truncated Fourier expansion of dependent variables and loading. Significant effect of material properties was also demonstrated by comparison of coupled and uncoupled results. Owing to the robustness of Fourier Finite Element method for axisymmetric problems with nonsymmetric loading and its capability to take low computation

costs, hereunto some authors used the method to solve Poisson’s equation in axisymmetric domain with singular edges [27, 28]. A novel mixed numerical method containing FE method and Fourier series proposed by Bakr et al [29] to simulate full 3D geophysical marine controlled source electromagnetic (CSEM) measurements. The main object of this paper was to overcome excessive time and memory requirements of direct matrix solver by reducing the dimensionality of the problem. Generally, in the discrete Fourier transform technique we deal with the list of coefficients of a finite combination of complex sinusoids. 3-D discretization of an axisymmetric body with application of discrete Fourier transform and finite element analyses was performed by Lai and Booker [30] to study of rigid caissons founded in both elastic and elasto-plastic soils. In contrast to the continues Fourier series approach, the discrete Fourier series representation overcome problems such as Gibbs phenomenon [30]. By doing a vast review on literature it is observed that the thermo-elastic analysis of functionally graded shells of revolution using hybrid FFT-FE method is scarce. Until now, Just the transient thermo-elastic analysis of disk brake has been studied using the fast Fourier transform and finite element method [31-33]. Currently, a modified Fourier series solution is developed for vibration analysis of shells of revolution by Jin et al [34, 35]. Mohazzab and Dozio [36, 37] used the spectral collocation method for prediction of natural frequencies of laminated curved panels and skew plates, respectively. The spectral collocation method based on integrated orthogonal polynomials was applied to the free vibration analysis of coupled axisymmetric laminated shell structures with arbitrary elastic-support boundary conditions (BCs) by Xie et al [38].

In this paper, the thermo-mechanical analysis of the proposed problem is done in following steps. At first, the heat conduction equation of an FG hollow cylinder is discretized using FFT technique in the periodic circumferential direction. It reduces two-dimensional partial differential governing equations (PDGE) including boundary conditions for a long cylinder into 1-D PDGE. Reduced boundary value problem is then analyzed using finite element method. The obtained results are in Fourier space and are imported as inputs for thermo-elastic analysis. In the next step, the thermo-elastic PDGEs of an FG hollow cylinder are solved in Fourier space by using Finite Element method. Afterwards, the obtained results are inverted into the real space through inverse Fast Fourier Transform technique. Non-symmetric pressure distribution is considered and results are compared with complete FE solution. In the sequel, thermo-elastic analysis of a hollow FG cylinder is successfully carried out using FFT-FE method.

2 FORMULATIONS

2.1 Heat conduction problem

At first, the steady state equation of heat conduction for an FG hollow cylinder in the absence of heat generation is considered. This equation is recognized as Laplace relationship and can be easily derived from Fourier law. Two-dimensional equation of heat conduction is considered here. Hence, the spatial domain in axial direction of cylinder is neglected. The steady state form of Laplace equation and related Dirichlet boundary conditions for an FG cylinder is written as follow [9]

$$\lambda_r \frac{\partial^2 T}{\partial r^2} + \frac{1}{r} \lambda_r \frac{\partial T}{\partial r} + \lambda_r \frac{1}{r^2} \frac{\partial^2 T}{\partial \theta^2} + \frac{d \lambda_r}{dr} \frac{\partial T}{\partial r} = 0 \quad a \leq r \leq b, \quad 0 < \theta \leq 2\pi, \tag{1}$$

$$\begin{aligned} T(r = a, \theta) &= T_i(\theta) \\ T(r = b, \theta) &= T_o(\theta) \end{aligned} \tag{2}$$

In which T is the temperature related to the initial conditions and $\lambda_r = \lambda_r(\bar{r})$ is the thermal conductivity coefficient. T_i and T_o are the distributed temperature at inner and outer surfaces of the cylinder. a and b are the inner and outer radius of the cylinder respectively. Here, the thermal conduction coefficient, $\lambda_r(\bar{r})$, is considered to be of the thickness of cylinder as:

$$\lambda_r = \lambda_{r0} \bar{r}^{m_1}, \quad \bar{r} = \frac{r-a}{b-a} \tag{3}$$

where, λ_{r0} is material constant and m_1 is the power law index of the material. As mentioned previously, the boundary conditions can be considered the periodic functions in terms of circumferential variable. Now, Fourier transform is used to solve this partial differential equation. For this purpose, the temperature field in Eq. (1) is replaced by the approximation function including finite Fourier coefficients. As shown in Fig. 1, the temperature field is defined at the discrete points θ_k which $k = 1, 2, \dots, N$. Points k in the circumferential direction show the number of harmonics in Fourier space. The selected approximation function is

$$T(r, \theta) = \sum_{k=1}^N \hat{T}_k(r) e^{ik\theta} \quad (4)$$

By substituting this relation into Eq. (1), the heat equation and its related boundary conditions in the radial direction are;

$$\frac{d^2 \hat{T}_k}{dr^2} + \frac{1}{r} \frac{d \hat{T}_k}{dr} + \frac{\lambda_r'}{\lambda_r} \frac{d \hat{T}_k}{dr} - \frac{k^2}{r^2} \hat{T}_k = 0 \quad \text{For } k=1, \dots, N \quad (5)$$

$$B.C \begin{cases} \hat{T}_k(r = a, \theta_k) = \hat{T}_i(\theta_k) \\ \hat{T}_k(r = b, \theta_k) = \hat{T}_o(\theta_k) \end{cases} \quad (6)$$

where the $(...)'$ denotes the first derivative of any arbitrary function with respect to r . Now, the weighted residuals method can appropriately provide a framework for solving this equation. A general form of the weighted residuals method is typically

$$\tilde{\Gamma}(\hat{T}_k(r)) - f = R \quad (7)$$

In general, approximate solution, \hat{T}_k , does not exactly satisfy Eq. (5). Thus, the weighted residual method is utilized to find the solution, so that the residual R , is to be minimized in the weighted integral scheme

$$\int_{\Omega^e} w R d\Gamma = 0 \quad (8)$$

where $d\Gamma = r dr$. Substituting Eq. (7) into Eq. (8) yields

$$\int_{\Omega^e} w_i \left[\frac{1}{r} \frac{d}{dr} \left(r \frac{d \hat{T}_k}{dr} \right) + \frac{\lambda_r'}{\lambda_r} \frac{d \hat{T}_k}{dr} - \frac{k^2}{r^2} \hat{T}_k \right] r dr = 0 \quad \text{For } k=1, \dots, N, \quad i=1, 2, \dots, N_r \quad (9)$$

Considering w_i as the sufficiently differentiable weight functions, the original equation can be easily transformed into the weak form using integration by parts technique as follows:

$$\int_{\Omega^e} \left[\frac{dw_i}{dr} r \frac{d \hat{T}_k}{dr} + \frac{k^2}{r} w_i \hat{T}_k - r \frac{\lambda_r'}{\lambda_r} \frac{d \hat{T}_k}{dr} w_i \right] dr - \left[\int_{\Gamma^e} w_i q_n ds \right] = 0 \quad (10)$$

where $q_n = r \left(\frac{d \hat{T}_k}{dr} n_r \right)$. In the radial direction, Eq. (10) is discretized by using the finite elements where j th element is located at the region $r_{j-1} \leq r \leq r_j$ (Fig. 1). The field variable, $\hat{T}_k(r)$, is then approximated by a combination of basic functions, ϕ_j^e and nodal values as:

$$\hat{T}_k^e(r) = \sum_{j=1}^{N_r} \phi_j^e(r) (\hat{T}_k^e)_j \tag{11}$$

where $(\hat{T}_k^e)_j$ are the nodal values of temperature field in the Fourier space. Based on the Babnov-Galerkin method, the weight functions, w_i , are considered to be the same as basic functions. Hence, by substituting Eq. (11) into the Eq. (10), governing equations become

$$\sum_{j=1}^{N_r} \int_{\Omega_e} \underbrace{\left(r \frac{d\phi_i^e}{dr} \frac{d\phi_j^e}{dr} + \frac{k^2}{r} \phi_i^e \phi_j^e - r \frac{\lambda_r'}{\lambda_r} \phi_i^e \frac{d\phi_j^e}{dr} \right) dr}_{\hat{K}_j^e} \hat{T}_j^e - \underbrace{\int_{\Gamma^e} \phi_i^e q_n ds}_{\hat{Q}_i^e} = 0 \tag{12}$$

It should be noted that in this paper we deal with the essential thermal boundary conditions. In order to determine the above integrals, the entire terms should be mapped into the parametric space. So, the basis functions are considered in terms of the auxiliary coordinate ξ as followings:

$$\begin{cases} \varphi_1 = \frac{1}{2}(1-\xi) \\ \varphi_2 = \frac{1}{2}(1+\xi) \end{cases} \tag{13}$$

Here, the iso-parametric approximation is used for describing the geometry of the spatial domain. In this scheme, the order of the solution and geometric approximations are the same, so it yields

$$r = \sum_{j=1}^m r_j^e \varphi_j^e(\xi) = [r_1 \quad r_2 \quad \dots \quad r_m] [\varphi_1 \quad \varphi_2 \quad \dots \quad \varphi_m]^T \tag{14}$$

$$\frac{\partial r}{\partial \xi} = \sum_{j=1}^m r_j^e \frac{\partial \varphi_j^e(\xi)}{\partial \xi} = [r_1 \quad r_2 \quad \dots \quad r_m] \left[\frac{\partial \varphi_1}{\partial \xi} \quad \frac{\partial \varphi_2}{\partial \xi} \quad \dots \quad \frac{\partial \varphi_m}{\partial \xi} \right]^T \tag{15}$$

Using geometric approximations of Eqs. (14) and (15), the governing equation for heat conduction in long cylinder can be solved numerically. The numerical integration needs to be performed for obtaining the stiffness matrix in parametric space. For this purpose, the Gauss-Legendre Quadrature method is used. Finally, the discretized heat equation in cylindrical coordinate is arranged in matrix form. By solving this set of equations, the nodal temperatures at each harmonic can be obtained, so we have

$$[\hat{K}] \{ \hat{T}_k \} = \{ \hat{Q} \} \tag{16}$$

2.2 FFT-FE analysis of thermo-elastic problem

In this section, the mixed FFT-FE method is implemented for the thermo-elastic analysis of an FG hollow cylinder. For this purpose, it is assumed that the cylindrical shell is stress free at reference temperature (T_0) and then it operates in a thermal environment. Thermal loading rises together with mechanical constraints at the boundaries produce thermal stresses in the cylinder. In order to derive the PDGEs of the cylindrical shell with assumed boundary conditions, the principle of virtual work in conjunction with the plane strain theory of elasticity is considered. The principle of virtual work which has been widely used in the large body of literatures is applicable to any continuous body with arbitrary constitutive behavior (i.e., elastic or inelastic). A special case of the principle of virtual work that deals with elastic mediums is known as the principle of minimum total potential energy and takes the form

$$\delta\Pi = \delta(V + U) = 0 \quad (17)$$

where δ is the variation symbol and Π is called the total potential energy of the elastic body. The strain energy (U) and energy of the applied loads (V) can be expressed as follows:

$$U = \frac{1}{2} \iiint_V \sigma_{ij} \varepsilon_{ij} dV \quad (18)$$

$$V = -\iint_{\Gamma} u_r \{r\sigma_{rr}n_r + \sigma_{r\theta}n_\theta\} ds - \iint_{\Gamma} u_\theta \{r\sigma_{r\theta}n_r + \sigma_{\theta\theta}n_\theta\} ds$$

By substituting Eq. (18) into Eq. (17) the non-vanishing terms contain

$$\delta\Pi = \iiint_V [\sigma_{rr}\delta\varepsilon_{rr} + \sigma_{\theta\theta}\delta\varepsilon_{\theta\theta} + 2\sigma_{r\theta}\varepsilon_{r\theta}] r dr d\theta \quad (19)$$

$$- \iint_{\Gamma} \delta u_r \{r\sigma_{rr}n_r + \sigma_{r\theta}n_\theta\} ds - \iint_{\Gamma} \delta u_\theta \{r\sigma_{r\theta}n_r + \sigma_{\theta\theta}n_\theta\} ds = 0$$

The kinematic relationship between the strain components and displacement field are defined as:

$$\varepsilon_{rr} = \frac{\partial u_r}{\partial r}, \quad \varepsilon_{\theta\theta} = \frac{1}{r} \left(u_r + \frac{\partial u_\theta}{\partial \theta} \right) \quad (20)$$

$$\varepsilon_{r\theta} = \frac{1}{2} \left(\frac{1}{r} \frac{\partial u_r}{\partial \theta} + \frac{\partial u_\theta}{\partial r} - \frac{u_\theta}{r} \right), \quad \varepsilon_{zz} = \varepsilon_{rz} = \varepsilon_{\theta z} = 0,$$

where ε_{ij} , ($i, j = r, \theta, z$) are the strain components in cylindrical coordinate. u_r and u_θ are displacement components in radial and circumferential directions, respectively. The plane strain linear thermo-elastic constitutive relations for an isotropic cylindrical shell can be written as:

$$\begin{Bmatrix} \sigma_{rr} \\ \sigma_{\theta\theta} \\ \sigma_{zz} \end{Bmatrix} = \begin{bmatrix} C_{11} & C_{12} & C_{13} \\ C_{21} & C_{22} & C_{23} \\ C_{31} & C_{32} & C_{33} \end{bmatrix} \begin{Bmatrix} \varepsilon_{rr} - \alpha\Delta T \\ \varepsilon_{\theta\theta} - \alpha\Delta T \\ \varepsilon_{zz} - \alpha\Delta T \end{Bmatrix}, \quad (21)$$

$$\sigma_{r\theta} = 2c_{44}\varepsilon_{r\theta}, \quad \sigma_{\theta z} = \sigma_{rz} = \varepsilon_{zz} = 0$$

where σ_{ij} , ($i, j = r, \theta, z$) are components of the cylindrical stress tensor. α is the coefficient of thermal expansion, $\Delta T (=T - T_0)$ is the temperature rise, and T_0 is the reference temperature at which the shell is stress free. The elastic constant coefficients C_{ij} , ($i, j = 1, 2, 3$) in terms of Young's modulus and Poisson's ratio are given as:

$$C_{11} = C_{22} = C_{33} = \lambda + 2\mu \quad (22)$$

$$C_{12} = C_{13} = C_{23} = \lambda, \quad C_{44} = \mu$$

where $\lambda = \frac{E\nu}{(1-2\nu)(1+\nu)}$, $\mu = \frac{E}{2(1+\nu)}$. In this work, we deal with FG cylinder in which the material properties are considered to be graded along the thickness (r -direction). So, the modulus of elasticity and coefficient of thermal expansion are assumed as following:

$$E(\bar{r}) = E_0 \bar{r}^{m_2}, \quad \alpha(\bar{r}) = \alpha_0 \bar{r}^{m_3} \quad (23)$$

where, E_0 and α_0 indicate the material constants and m_2 and m_3 are the power law indices of the material. Substituting Eqs. (20) – (22) into the Eq. (19) yields the following integral form

$$\begin{aligned} & \iint \left\{ \left[\lambda \left(\frac{\partial u_r}{\partial r} + \frac{u_r}{r} + \frac{1}{r} \frac{\partial u_\theta}{\partial \theta} \right) + 2\mu \frac{\partial u_r}{\partial r} - (3\lambda + 2\mu)\alpha\Delta T \right] \frac{\partial w_1}{\partial r} \right. \\ & + \left[\lambda \left(\frac{\partial u_r}{\partial r} + \frac{u_r}{r} + \frac{1}{r} \frac{\partial u_\theta}{\partial \theta} \right) + 2\mu \left(\frac{u_r}{r} + \frac{1}{r} \frac{\partial u_\theta}{\partial \theta} \right) - (3\lambda + 2\mu)\alpha\Delta T \right] \left(\frac{w_1}{r} + \frac{1}{r} \frac{\partial w_2}{\partial \theta} \right) \\ & \left. + \mu \left(\frac{1}{r} \frac{\partial u_r}{\partial \theta} + \frac{\partial u_\theta}{\partial r} - \frac{u_\theta}{r} \right) \left(\frac{1}{r} \frac{\partial w_1}{\partial \theta} + \frac{\partial w_2}{\partial r} - \frac{w_2}{r} \right) \right\} r dr d\theta = 0 \end{aligned} \tag{24}$$

In general, two sets of partial differential governing equations can be extracted for thermo-elastic analysis of the FG cylinder. In continuum mechanics of a solid, the first variation of the energy functional yields a weak form of the governing equations as a bilinear form. w_1, w_2 in above equation, represent the variations of displacement components in the radial and circumferential directions, respectively. Using the integration by parts technique with respect to the radial and circumferential spatial variables (r, θ) , the following sets of governing equations for a homogeneous isotropic elastic solid are obtained,

$$\begin{aligned} & \mu(\nabla^2 u_r - \frac{u_r}{r^2} - \frac{2}{r^2} \frac{\partial u_\theta}{\partial \theta}) + (\lambda + \mu) \frac{\partial}{\partial r} \left(\frac{1}{r} \frac{\partial}{\partial r} (ru_r) + \frac{1}{r} \frac{\partial u_\theta}{\partial \theta} \right) + (3\lambda + 2\mu)\alpha \left[\frac{\partial (r\Delta T)}{\partial r} - \Delta T \right] = 0 \\ & \mu(\nabla^2 u_\theta - \frac{u_\theta}{r^2} - \frac{2}{r^2} \frac{\partial u_r}{\partial \theta}) + (\lambda + \mu) \frac{1}{r} \frac{\partial}{\partial \theta} \left(\frac{1}{r} \frac{\partial}{\partial r} (ru_r) + \frac{1}{r} \frac{\partial u_\theta}{\partial \theta} \right) + (3\lambda + 2\mu)\alpha \frac{\partial (\Delta T)}{\partial \theta} = 0 \end{aligned} \tag{25}$$

where $\nabla^2 u_r = \frac{1}{r} \frac{\partial}{\partial r} \left(r \frac{\partial u_r}{\partial r} \right) + \frac{1}{r^2} \frac{\partial^2 u_r}{\partial \theta^2}$.

The corresponding boundary conditions are as follow:

$$\begin{aligned} & \int_{\Gamma} w_1 \left\{ \left[\lambda r \left(\frac{\partial u_r}{\partial r} + \frac{u_r}{r} + \frac{1}{r} \frac{\partial u_\theta}{\partial \theta} \right) + 2\mu r \frac{\partial u_r}{\partial r} \right] n_r + \left[\mu \left(\frac{1}{r} \frac{\partial u_r}{\partial \theta} + \frac{\partial u_\theta}{\partial r} - \frac{u_\theta}{r} \right) \right] n_\theta \right\} ds = \int_{\Gamma} w_1 \{ r\sigma_r n_r + \sigma_{r\theta} n_\theta \} ds \\ & \int_{\Gamma} w_2 \left\{ \left[\mu r \left(\frac{1}{r} \frac{\partial u_r}{\partial \theta} + \frac{\partial u_\theta}{\partial r} - \frac{u_\theta}{r} \right) \right] n_r + \left[\lambda \left(\frac{\partial u_r}{\partial r} + \frac{u_r}{r} + \frac{1}{r} \frac{\partial u_\theta}{\partial \theta} \right) + 2\mu \left(\frac{u_r}{r} + \frac{1}{r} \frac{\partial u_\theta}{\partial \theta} \right) \right] n_\theta \right\} ds = \int_{\Gamma} w_2 \{ r\sigma_{r\theta} n_r + \sigma_{\theta\theta} n_\theta \} ds \end{aligned} \tag{26}$$

Mutually, FFT-FE method can be used to discretize the thermo-elastic governing equations of the FG cylinder. At first, the Fourier transform is used to discretize the PDGEs into a set of harmonics. For this purpose two sets of approximation functions are considered for displacement components. Based on the FFT technique, these functions can be selected as:

$$\begin{cases} u_r(r, \theta) = \sum_{k=1}^N \hat{u}_r^k(r) e^{ik\theta} \\ u_\theta(r, \theta) = \sum_{k=1}^N \hat{u}_\theta^k(r) e^{ik\theta} \end{cases} \tag{27}$$

where \hat{u}_r^k and \hat{u}_θ^k are the displacement components in Fourier space. Substituting the approximation functions of Eq. (27) into Eq. (24), two sets of governing equations and their related boundary conditions in the weak form are obtained as follow:

$$\begin{aligned}
& \int \left\{ \frac{dw_1}{dr} \left[\lambda \left(\hat{u}_r^k + r \frac{d\hat{u}_r^k}{dr} + ik\hat{u}_\theta^k \right) + 2\mu r \frac{d\hat{u}_r^k}{dr} - (3\lambda + 2\mu)r\alpha \left(\Delta\hat{T}_k \right) \right] \right. \\
& + w_1 \left[\lambda \left(\frac{\hat{u}_r^k}{r} + \frac{d\hat{u}_r^k}{dr} + \frac{ik}{r}\hat{u}_\theta^k \right) + 2\mu \left(\frac{\hat{u}_r^k}{r} + \frac{ik}{r}\hat{u}_\theta^k \right) - (3\lambda + 2\mu)\alpha \left(\Delta\hat{T}_k \right) \right. \\
& \left. \left. + \mu \left(\frac{k^2}{r}\hat{u}_r^k - ik \frac{d\hat{u}_\theta^k}{dr} + \frac{ik}{r}\hat{u}_\theta^k \right) \right] \right\} dr - \underbrace{\int_{\Gamma} w_1 \left[\lambda \left(\hat{u}_r^k + r \frac{d\hat{u}_r^k}{dr} + ik\hat{u}_\theta^k - 3r\alpha \left(\Delta\hat{T}_k \right) \right) + 2\mu \left(r \frac{d\hat{u}_r^k}{dr} - r\alpha \left(\Delta\hat{T}_k \right) \right) \right]}_{r\hat{\sigma}_r} n_r ds = 0
\end{aligned} \tag{28}$$

$$\begin{aligned}
& \int \left\{ \frac{dw_2}{dr} \left[\mu \left(r \frac{d\hat{u}_\theta^k}{dr} - \hat{u}_\theta^k + ik\hat{u}_r^k \right) \right] + w_2 \left[\mu \left(\frac{2k^2}{r}\hat{u}_\theta^k + \frac{\hat{u}_\theta^k}{r} - \frac{d\hat{u}_\theta^k}{dr} - \frac{3ik}{r}\hat{u}_r^k \right) \right. \right. \\
& \left. \left. - \lambda \left(\frac{1}{r} \frac{d}{dr} (rik\hat{u}_r^k) - \frac{k^2}{r}\hat{u}_\theta^k \right) + (3\lambda + 2\mu)\alpha ik \left(\Delta\hat{T}_k \right) \right] \right\} dr - \underbrace{\int_{\Gamma} w_2 \left[\mu \left(r \frac{d\hat{u}_\theta^k}{dr} - \hat{u}_\theta^k + ik\hat{u}_r^k \right) \right]}_{r\hat{\tau}_{\theta}} n_r ds = 0
\end{aligned} \tag{29}$$

Now, this set of equations can be solved for each harmonic in Fourier space. As shown in Fig. 1, two displacement components as the nodal degrees of freedom are considered at discrete points θ_k , ($k=1, 2, \dots, N$). Furthermore, the governing equations at each harmonic are discretized by using FE approach. Hence, the following linear approximations are considered to estimate displacement components in the Fourier space.

$$\begin{Bmatrix} \hat{u}_r^k \\ \hat{u}_\theta^k \end{Bmatrix}^e = \begin{bmatrix} \phi_1 & \phi_2 & 0 & 0 \\ 0 & 0 & \phi_1 & \phi_2 \end{bmatrix} \begin{Bmatrix} \left(\hat{u}_r^k \right)_1 \\ \left(\hat{u}_r^k \right)_2 \\ \left(\hat{u}_\theta^k \right)_1 \\ \left(\hat{u}_\theta^k \right)_2 \end{Bmatrix}^e \tag{30}$$

where ϕ_j are linear basis functions presented in Eq. (13). Additionally, $\left(\hat{u}_r^k \right)_j$ and $\left(\hat{u}_\theta^k \right)_j$ are the radial and circumferential displacement nodal values in Fourier space, respectively. Consequently, substituting the FE approximations functions of Eq. (30) into Eqs. (28) and (29) and using the geometric approximations of Eq. (14) and (15) yield

$$\begin{bmatrix} \left[\hat{K}^{11} \right] & \left[\hat{K}^{12} \right] \\ \left[\hat{K}^{21} \right] & \left[\hat{K}^{22} \right] \end{bmatrix} \begin{Bmatrix} \left\{ \hat{u}_r \right\} \\ \left\{ \hat{u}_\theta \right\} \end{Bmatrix} = \begin{Bmatrix} \left\{ \hat{F}^1 \right\} \\ \left\{ \hat{F}^2 \right\} \end{Bmatrix} - \begin{bmatrix} \left[\hat{G}^{11} \right] & 0 \\ 0 & \left[\hat{G}^{22} \right] \end{bmatrix} \begin{Bmatrix} \left\{ \Delta\hat{T} \right\} \end{Bmatrix} \tag{31}$$

where $\left\{ \hat{u}_r \right\} = \left[\left(\hat{u}_r^k \right)_1 \quad \left(\hat{u}_r^k \right)_2 \right]^T$, $\left\{ \hat{u}_\theta \right\} = \left[\left(\hat{u}_\theta^k \right)_1 \quad \left(\hat{u}_\theta^k \right)_2 \right]^T$, $\left\{ \Delta\hat{T} \right\} = \left[\left(\Delta\hat{T}_k \right)_1 \quad \left(\Delta\hat{T}_k \right)_2 \right]^T$.

The elements of $\left[\hat{K}^{(mn)} \right]$, $\left[\hat{G}^{(mm)} \right]$ and $\left\{ \hat{F}^m \right\}$ are given in Appendix. Foregoing matrix equation can successfully represent the equilibrium state of an element from local aspect and entire body from global aspect. Therefore, the global stiffness and force matrices can be obtained using assembly technique. The output results from this equation are displacement nodal values in Fourier space. It is necessary to invert the obtaining results from complex (Fourier) space into the main real space. The Inverse Fast Fourier Transform (IFFT) technique can be effectively used for this end.

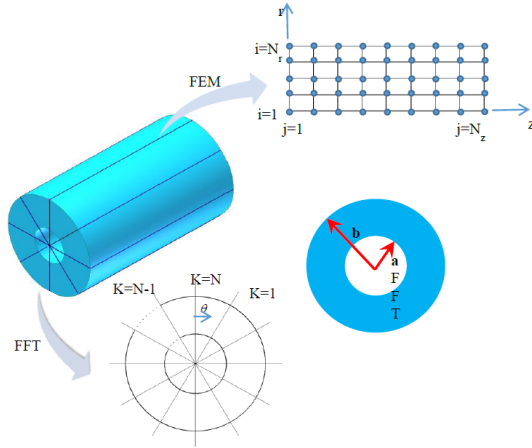


Fig.1
Geometrical configuration of finite elements and discrete FFT grids on cylindrical domain.

3 RESULTS AND DISCUSSION

To illustrate the convergence, accuracy and effectiveness of the suggested method, some numerical examples related to thermo-elastic analysis of the cylindrical shell are presented in this section. Thus, a comparison is separately made between responses of the present method and those of exact and FE solution. In order to verify the solution procedure, two sets of materials including FG and homogeneous materials (HM) are considered as follows:

$$\begin{aligned}
 m_1=m_2=m_3=0, \text{ (HM)}, a=0.2 \text{ (m)}, b=0.5 \text{ (m)}, E_0=210 \text{ (GPa)}, \nu=0.3, \alpha_0=12 \times 10^{-6} \text{ (1/}^\circ\text{C)} \\
 m_1=m_2=m_3=m, \text{ (FGM)}, a=1 \text{ (m)}, b=1.2 \text{ (m)}, E_0=200 \text{ (GPa)}, \nu=0.3, \alpha_0=1.2 \times 10^{-6} \text{ (1/}^\circ\text{C)}
 \end{aligned}$$

3.1 Convergence study (HM)

The heat conduction equation is now considered for investigating the rate of convergence in the present mixed method. Since, the present method is constructed using combining two different numerical methods; the convergence study should be performed separately. The adaptability of the combined proposed method for analyzing the thermo-elastic problem is clarified using the flow chart presented in Fig. 2. In spite of the fact that Fourier transform is recognized as an analytical method for solving boundary value problems, the FFT technique acts as a numerical that which can transform the finite data from a real domain into the complex one. In this work, the blocked code in MATLAB software is used to Fourier transform and inverting vice versa [39]. For the convergence study, the following formula can be used to extract the relative error of the obtained results.

$$\text{Error\%} = \left\| \frac{\text{Present solution-Exact solution}}{\text{Exact solution}} \right\| \times 100 \tag{32}$$

The heat conduction of a cylinder with uniform boundary temperature at the inner surface, T_i , and the outer surface, T_o , is selected as a case study. Thereafter, the fast Fourier transform and finite element discretization are accomplished on the heat equation. In order to extract the relative error, obtained results are compared with those of extracted from the exact solution [40]. In Fig. 3 the convergence of results with respect to element mesh sizes is shown. It is observed from the figure that by increasing the element numbers in the radial direction the results converge smoothly as a straight line. This kind of convergence study is known as h -version technique in which the density of linear elements is raised until the desired precision is achieved. In Fig. 4 the convergence behavior of the FFT method is shown for some periodic functions. These functions are assumed to be the boundary conditions of the inner surface of the cylinder. As shown, the rate of convergence regarding fast Fourier transform technique is affected by increasing the wave number in periodic functions. For $T(\theta) = \sin(\theta)$, the method can appropriately attain the machine precision in the finite harmonics as expected. In spite of the linear behavior observed from FE convergence study, Fig. 4 shows an exponentially varying behavior of relative error. This difference between two

logarithmic scaled graphs depicts that FFT is more vigorous and accurate than FEM for analyzing the problems with periodic domain.

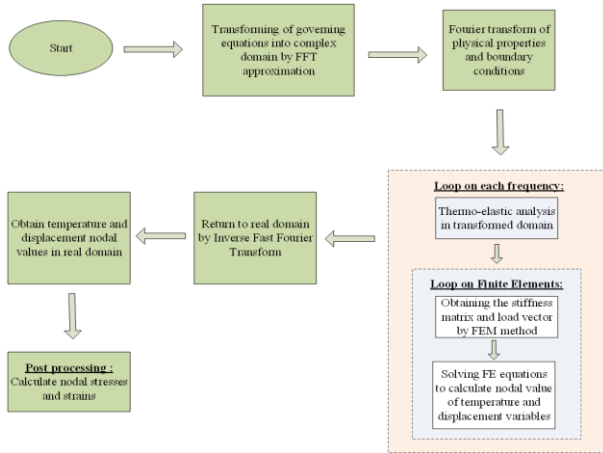


Fig.2 Hybrid FFT-FE approach in thermo-mechanical analysis flow chart.

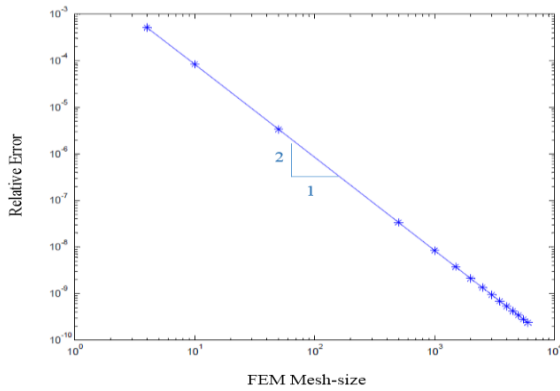


Fig.3 Logarithmic representation of relative error versus FEM mesh-size increasing.

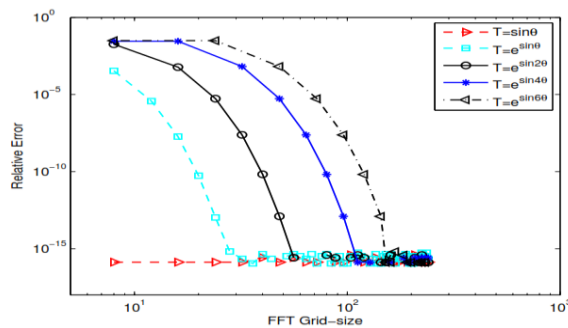


Fig.4 Logarithmic representation of relative error versus FFT Grid-size.

3.2 Validation for HM and FGM

3.2.1 Elasto-static analysis

In the previous section, conformability and convergence of the two mentioned methods was investigated separately. Here, the finite element commercial code in ABAQUS software is used to validate the obtained results. Initially, the entire hollow HM cylinder is modeled in part module and the corresponding material properties and boundary conditions were assigned respectively. Appropriate mesh with CPE4R label is defined for this analysis. The inner surface of hollow cylinder was fully clamped with respect to predefined degrees of freedom. Mutually, the periodic pressure, $P = 5 \times 10^6 \sin(2\theta + 1)$, was considered to act on outer surface of the hollow cylinder. Nodal values of radial displacement component, u_r , which are extracted for middle surface of the hollow cylinder, are presented in

Fig. 5 and Fig. 6. For better demonstration, both of the FFT-FE and complete FE results are presented in these figures. It can be observed that the present mixed method is in good agreement with the complete FE solution. In Fig. 6, the mesh refinement is considered for the ABAQUS model. In this case, the element density of the model is raised up to two times. It is obvious that the complete FE results are dramatically tracing the present FFT-FE solution.

In Fig. 7 the results of circumferential displacement, u_{θ} , for the interval $[0,2\pi]$ are presented. In Fig. 8, mesh refinement is employed for analyzing the cylinder using commercial FE code. According to Fig. 2, the post processing is performed upon the system of governing equations and nodal values of displacements are specified. The strain components need to be obtained in such a procedure. For this purpose, in Fourier space, the IFFT technique is implemented on strain components.

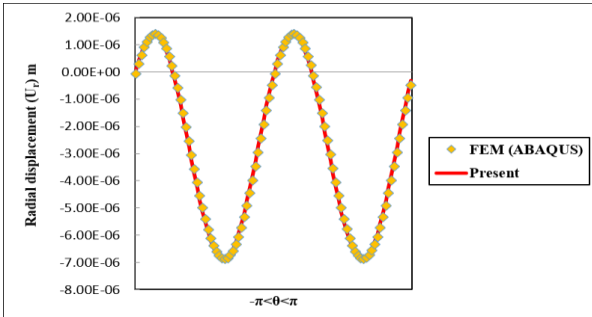


Fig.5
Radial displacement, U_r , in middle surface of cylinder considered at interval $[0,2\pi]$, ($N_{el}=500$, $N=200$).

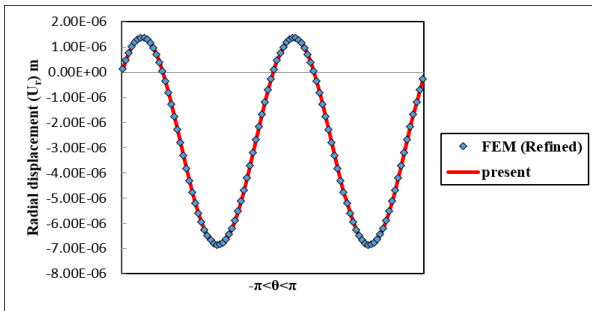


Fig.6
Radial displacement, U_r , in middle surface of cylinder considered at interval $[0,2\pi]$, ($N_{el}=500$, $N=200$).

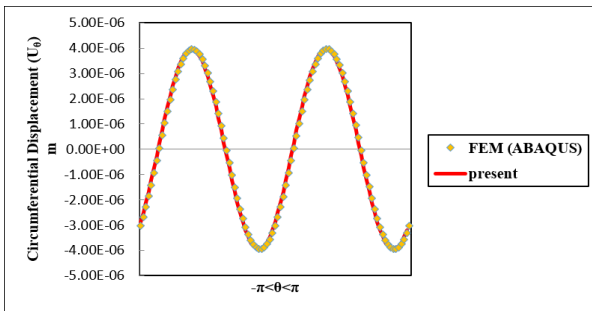


Fig.7
Circumferential displacement, U_{θ} , in the middle surface of the cylinder considered at interval $[0,2\pi]$, ($N_{el}=500$, $N=200$).

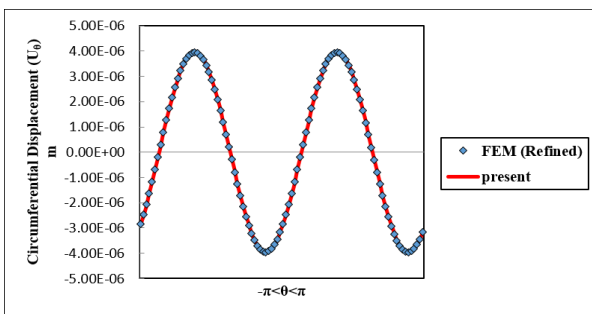


Fig.8
Circumferential displacement, U_{θ} , in the middle surface of the cylinder at interval $[0,2\pi]$, ($N_{el}=500$, $N=200$).

The influence of the mesh refinement is appropriately depicted in Fig. 9 and Fig. 10 for the radial strain component of the cylinder. Consequently, the results for circumferential and shear strain components are presented in Figs. 11-14. Hereunto, the validation of the hybrid FFT-FE method has been carried out for elasto-static analysis of hollow HM cylinder. Now, the results obtained from the thermo-elastic analysis are compared with those of extracted from exact solution [40] and are presented in Fig. 15. Degrees of freedom pertaining to the displacement field are fully clamped at inner and outer surfaces of the cylinder. A uniform distribution of temperature is considered at the inner, ($T_i=100\text{ }^\circ\text{C}$) and outer ($T_o=25\text{ }^\circ\text{C}$) surface of the hollow HM cylinder. Finally, the results of elasto-static analysis of a cylinder under harmonic pressure are presented as contour plots in Figs. 16-19.

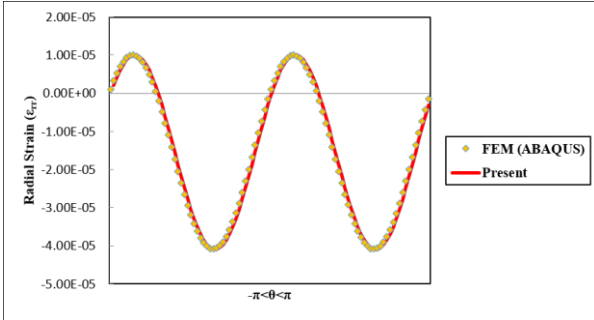


Fig.9 Strain component of the middle surface of hollow cylinder in the radial direction for interval $[0,2\pi]$, ($N_{el}=500$, $N=200$).

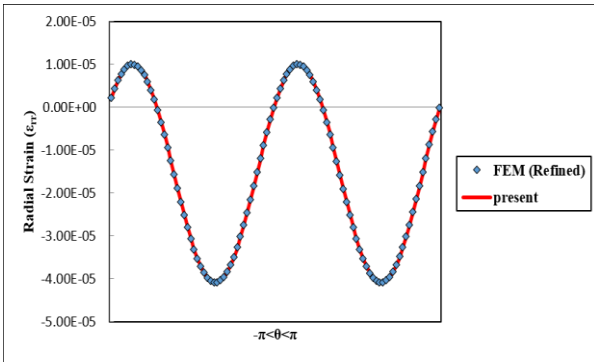


Fig.10 Strain component of the middle surface of hollow cylinder in the radial direction for interval $[0,2\pi]$, ($N_{el}=500$, $N=200$).

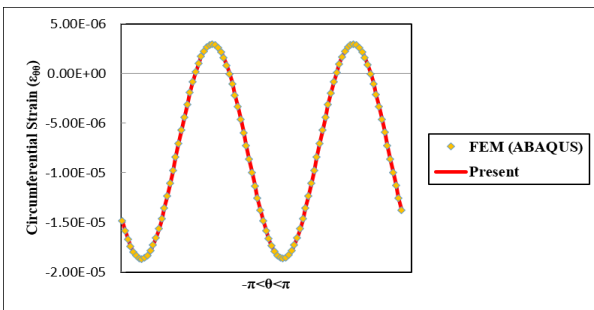


Fig.11 Strain component of the middle surface of hollow cylinder in the circumferential direction for interval $[0,2\pi]$, ($N_{el}=500$, $N=200$).

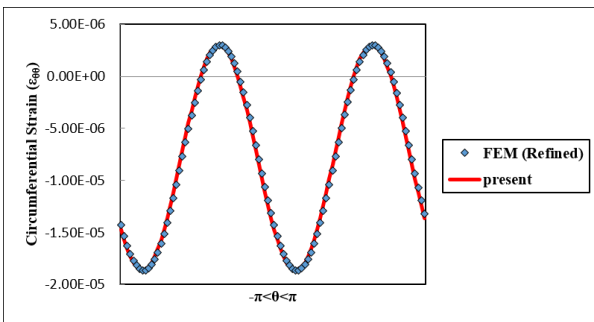


Fig.12 Strain component of the middle surface of hollow cylinder in the circumferential direction for interval $[0,2\pi]$, ($N_{el}=500$, $N=200$).

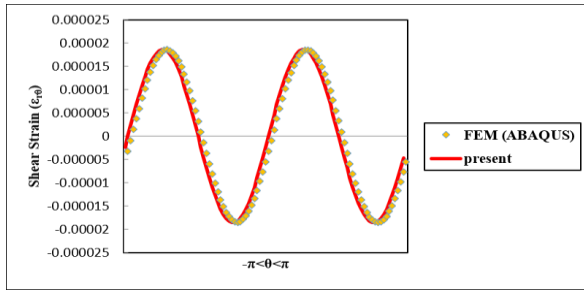


Fig.13 Shear strain of the middle surface of hollow cylinder for interval $[0,2\pi]$, ($N_{el}=500, N=200$).

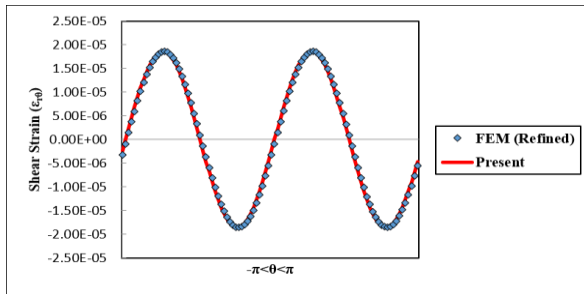


Fig.14 Shear strain of the middle surface of hollow cylinder for interval $[0,2\pi]$, ($N_{el}=500, N=200$).

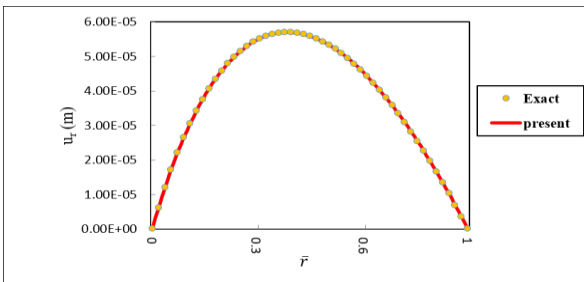


Fig.15 Axi-symmetric radial displacement, u_r , due to temperature variation.

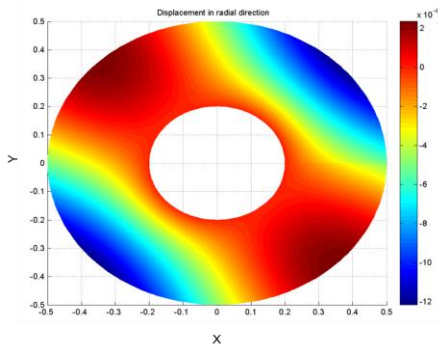


Fig.16 Contour plot of displacement component in radial direction, u_r , (m).

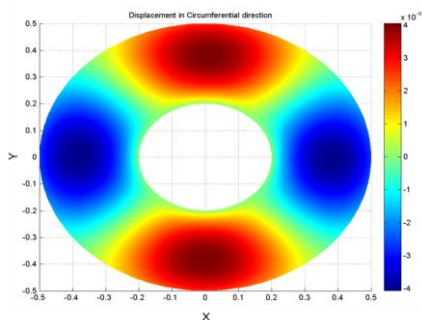


Fig.17 Contour plot of displacement component in circumferential direction, u_θ , (m).

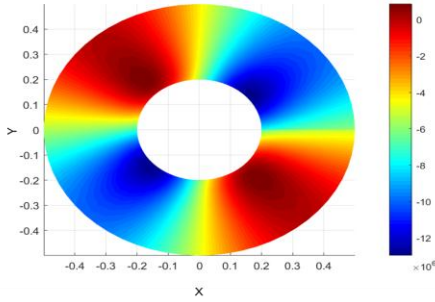


Fig.18
Contour plot of normal stress in radial direction, σ_{rr} , (Pa).

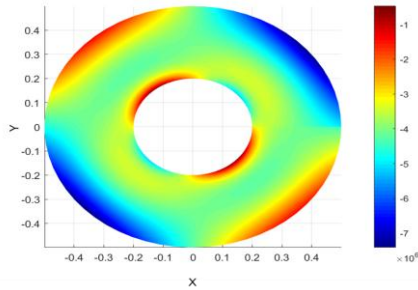


Fig.19
Contour plot of hoop stress component, $\sigma_{\theta\theta}$, (Pa).

3.2.2 Thermo-elastic demonstration

In this paper, the governing equations are derived for thermo-elastic analysis of a hollow FG cylinder. By considering the material properties chosen at the beginning of this section for the FG material, we can obtain the thermo-elastic response of a cylinder under various thermal and mechanical loading. As the first example, boundary conditions for thermal analysis are taken as $T(a) = 10^\circ\text{C}$ and $T(b) = 0^\circ\text{C}$. The uniform pressure is assumed to be applied at the inner surface of the cylinder. So, the boundary conditions for stresses can be represented as follows:

$$\sigma_r(a) = -50 \text{ MPa}, \quad \sigma_r(b) = 0 \text{ MPa} \quad (33)$$

Fig. 20 shows the comparison between temperature distribution obtained from the present mixed-method and the exact solution of Ref [2]. As shown in Fig. 21, the analytical solution for the radial displacement of the hollow FG cylinder in absence of thermal effects (Ref [10]) is appropriately followed by the present hybrid method. For various power-law indices of the FG material (m), the distributions of thermal stresses in the radial and circumferential directions are presented in Fig. 22 and Fig. 23 respectively. In the sequel, the periodic thermal and mechanical boundary conditions at the inner surface of the hollow FG cylinder are considered

$$\begin{aligned} T(a, \theta) &= 60 \cos(2\theta)^\circ\text{C} \\ \sigma_r(a, \theta) &= 0, \quad \sigma_{r\theta}(a, \theta) = 0 \\ u_r(b, \theta) &= 0, \quad u_\theta(b, \theta) = 0. \end{aligned} \quad (34)$$

2D distribution of the temperature field and the displacement components are shown in Figs. 24-26. A simple comparison indicates that the obtained results are in good agreement with the exact solution of Ref [3].

Obtaining analytical solutions for the problems with complex geometry and boundary conditions often is time-consuming and sometimes may be impossible. In such cases, the numerical techniques such as the FFT-FE method can be used to achieve an approximate solution of the problem. In this regards, thermo-mechanical responses of an FG cylinder whose half of the boundary is exposed to thermal loading are investigated here. The following boundary conditions are assumed for the hollow FG cylinder:

$$\begin{aligned}
 T(a, \theta) &= e^{5 \sin \theta} \text{ } ^\circ\text{C}, \quad T(b, \theta) = 60 \text{ } ^\circ\text{C}, \\
 u_r(a, \theta) &= 0, \quad u_\theta(a, \theta) = 0, \\
 u_r(b, \theta) &= 0, \quad u_\theta(b, \theta) = 0.
 \end{aligned}
 \tag{35}$$

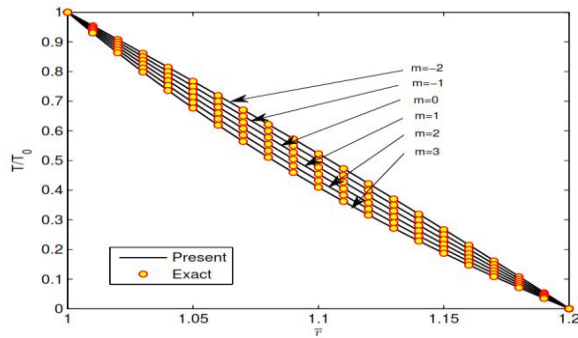


Fig.20
Temperature distributions along the thickness of cylinder.

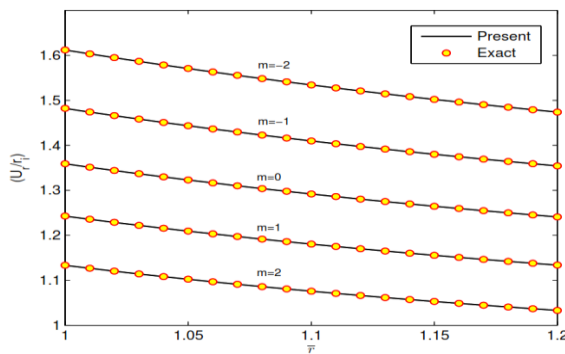


Fig.21
Distribution of radial displacement within the wall of the cylinder.

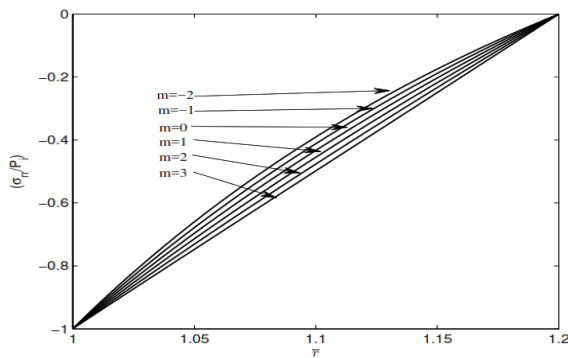


Fig.22
Variation of normal stress in the radial direction for inner pressurized cylinder.

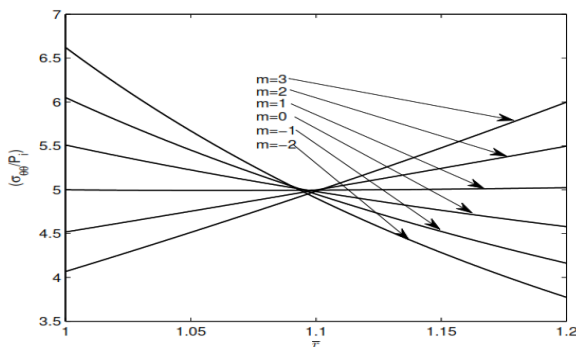


Fig.23
Variation of normal stress in the circumferential direction for inner pressurized cylinder.

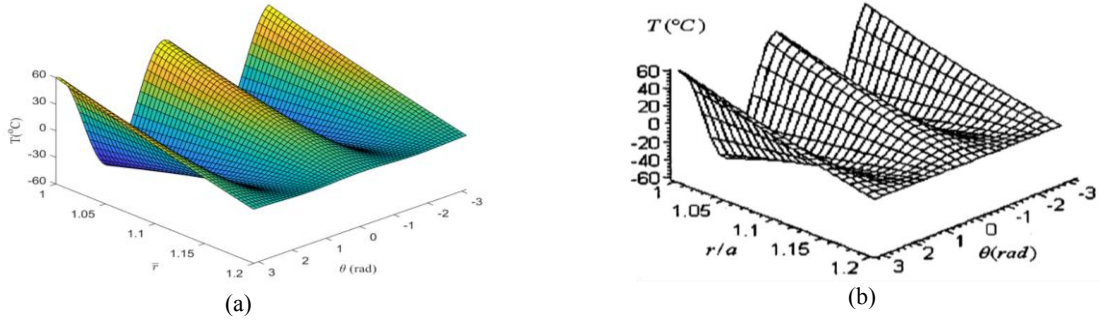


Fig.24
2D nonsymmetric distribution of the temperature across the cylinder section.

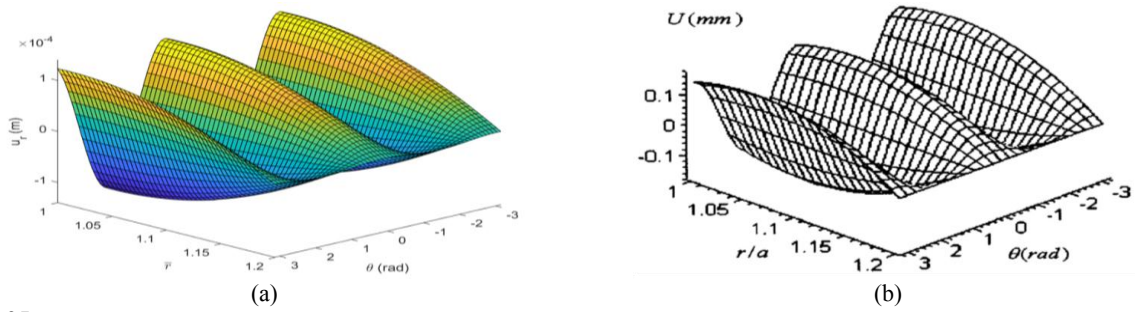


Fig.25
2D nonsymmetric distribution of radial displacement across the cylinder section.

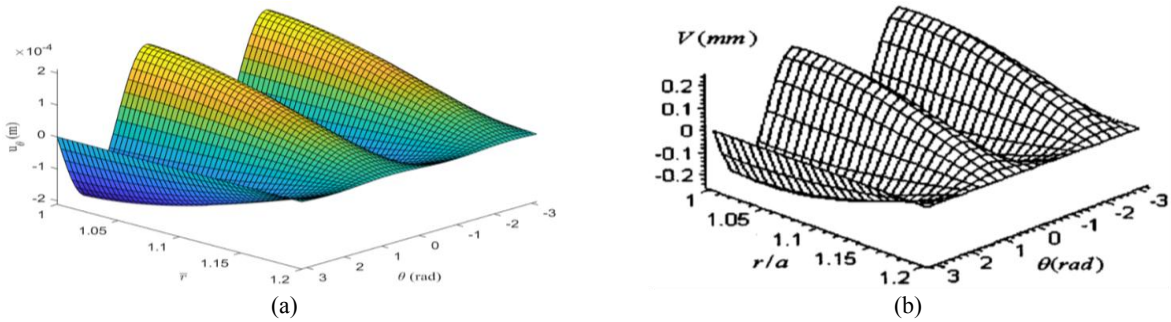


Fig.26
2D nonsymmetric distribution of circumferential displacement across the cylinder section.

Responses of this temperature excitation across the FG cylinder section are presented in Figs. 27-31.

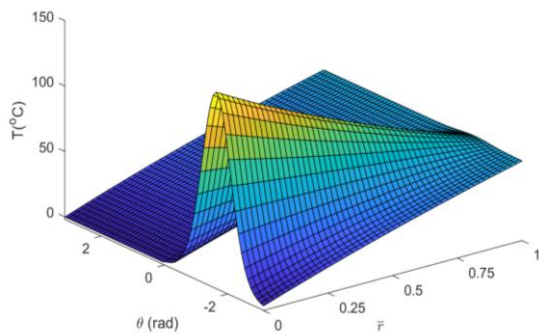


Fig.27
2D nonsymmetric distribution of the temperature in the cylinder section.

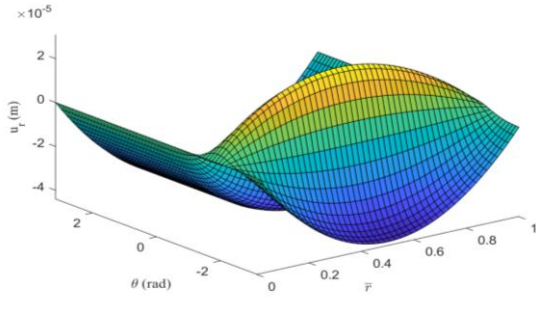


Fig.28
2D nonsymmetric distribution of the radial displacement in the cylinder section.

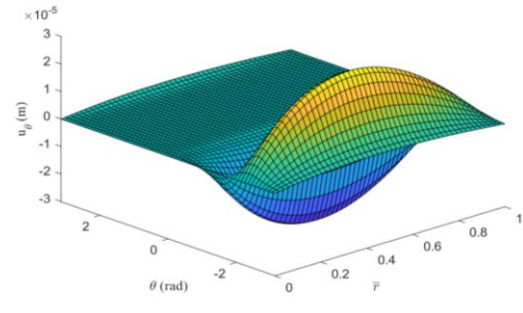


Fig.29
2D nonsymmetric distribution of the circumferential displacement in the cylinder section.

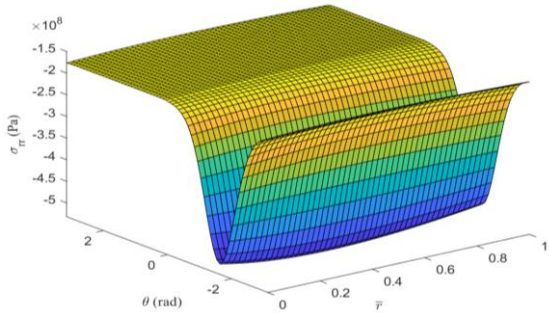


Fig.30
2D nonsymmetric distribution of the radial stress in the cylinder section.

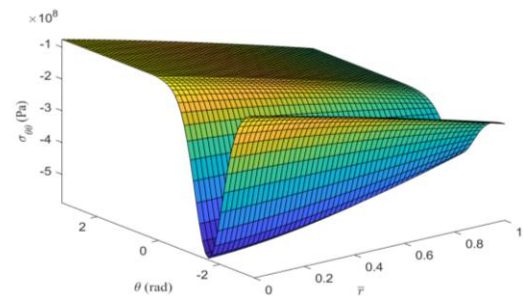


Fig.31
2D nonsymmetric distribution of the hoop stress in the cylinder section.

4 CONCLUSION

In this paper, a combination of fast Fourier transform technique and conventional finite element method was employed successfully for thermo-mechanical analysis of a hollow FG cylinder. In shells of revolution, we can suitably use Fourier transform in the circumferential direction. Hamilton's principle was used for deriving thermo-elastic governing equations of the FG cylinder. Discretization of equations and related boundary conditions was utilized using discrete Fourier transform in the circumferential direction. In the radial direction, the FE method was

used to solve PDGEs. The discrete transform can be computed with the $2N^2$ operations required by a matrix-vector multiplication. The fast Fourier transform technique which is successfully implemented in this paper has an operation count with leading term $(5/2)N \log_2 N$. In the numerical analyses, it is accompanied by a great time saving of computations. Asymmetric boundary conditions were considered and obtained results were validated using exact and complete FE solutions. The investigations showed that the present method is in good agreement with exact analytical solutions. In convergence study, the FFT technique showed much better behavior in comparison with the finite element method. It can be concluded that the FE mesh-sizes have more influence in convergence than FFT nodal density. The proposed method (FFT-FE) enjoys both the ability of FEM in modeling complicated geometry and the simplicity and accuracy of FFT. The present hybrid method can be extended to three-dimensional elasto-static and elasto-dynamic analysis of homogeneous, composite, and functionally graded thick shells of revolution.

APPENDIX A

$$\hat{K}_{ij}^{11} = \int_{\Omega^e} \left\{ \frac{d\phi_i}{dr} \left[\lambda \left(\phi_j + r \frac{d\phi_j}{dr} \right) + 2\mu r \frac{d\phi_j}{dr} \right] + \phi_i \left[\lambda \left(\frac{1}{r} \phi_j + \frac{d\phi_j}{dr} \right) + \mu \left(\frac{2}{r} \phi_j + \frac{1}{r} k^2 \phi_j \right) \right] \right\} dr \quad (\text{A.1})$$

$$\hat{K}_{ij}^{12} = \int_{\Omega^e} \left\{ \frac{d\phi_i}{dr} \lambda (ik \phi_j) + \phi_i \left[\frac{\lambda}{r} ik \phi_j + \mu \left(\frac{3}{r} ik \phi_j - ik \frac{d\phi_j}{dr} \right) \right] \right\} dr \quad (\text{A.2})$$

$$\hat{K}_{ij}^{21} = \int_{\Omega^e} \left\{ \frac{d\phi_i}{dr} \mu (ik \phi_j) + \phi_i \left[-\lambda \left(\frac{1}{r} ik \phi_j + ik \frac{d\phi_j}{dr} \right) - \frac{3\mu}{r} ik \phi_j \right] \right\} dr \quad (\text{A.3})$$

$$\hat{K}_{ij}^{22} = \int_{\Omega^e} \left\{ \frac{d\phi_i}{dr} \mu \left(r \frac{d\phi_j}{dr} - \phi_j \right) + \phi_i \left[\mu \left(\frac{2}{r} k^2 \phi_j + \frac{1}{r} \phi_j - \frac{d\phi_j}{dr} \right) + \lambda \frac{1}{r} k^2 \phi_j \right] \right\} dr \quad (\text{A.4})$$

$$\hat{G}_{ij}^{11} = - \int_{\Omega^e} \left\{ (3\lambda + 2\mu) \alpha \left[r \frac{d\phi_i}{dr} \phi_j + \phi_i \phi_j \right] \right\} dr \quad (\text{A.5})$$

$$\hat{G}_{ij}^{22} = \int_{\Omega^e} \left\{ (3\lambda + 2\mu) \alpha ik \phi_i \phi_j \right\} dr \quad (\text{A.6})$$

$$\hat{F}_i^1 = \int_{\Gamma^e} \phi_i (r \hat{\sigma}_r) ds \quad (\text{A.7})$$

$$\hat{F}_i^2 = \int_{\Gamma^e} \phi_i (r \hat{\tau}_{\theta r}) ds \quad (\text{A.8})$$

REFERENCES

- [1] Obata Y., Noda N., 1994, Steady thermal stresses in a hollow circular cylinder and a hollow sphere of a functionally graded material, *Journal of Thermal Stresses* **17**(3): 471-487.
- [2] Jabbari M., Sohrabpour S., Eslami M., 2002, Mechanical and thermal stresses in a functionally graded hollow cylinder due to radially symmetric loads, *International Journal of Pressure Vessels and Piping* **79**(7): 493-497.
- [3] Jabbari M., Sohrabpour S., Eslami M., 2003, General solution for mechanical and thermal stresses in a functionally graded hollow cylinder due to nonaxisymmetric steady-state loads, *Journal of Applied Mechanics* **70**(1): 111-118.
- [4] Ootao Y., Akai T., Tanigawa Y., 2008, Transient piezothermoelastic analysis for a functionally graded thermopiezoelectric hollow cylinder, *Journal of Thermal Stresses* **31**(10): 935-955.

- [5] Malekzadeh P., Heydarpour Y., 2012, Response of functionally graded cylindrical shells under moving thermo-mechanical loads, *Thin-Walled Structures* **58**: 51-66.
- [6] Moosaie A., 2012, Steady symmetrical temperature field in a hollow spherical particle with temperature-dependent thermal conductivity, *Archives of Mechanics* **64**(4): 405-422.
- [7] Moosaie A., 2015, Axisymmetric steady temperature field in FGM cylindrical shells with temperature-dependent heat conductivity and arbitrary linear boundary conditions, *Archives of Mechanics* **67**(3): 233-251.
- [8] Moosaie A., 2016, A nonlinear analysis of thermal stresses in an incompressible functionally graded hollow cylinder with temperature-dependent material properties, *European Journal of Mechanics-A/Solids* **55**: 212-220.
- [9] Dehghan M., Nejad M.Z., Moosaie A., 2016, Thermo-electro-elastic analysis of functionally graded piezoelectric shells of revolution: Governing equations and solutions for some simple cases, *International Journal of Engineering Science* **104**: 34-61.
- [10] Nejad M.Z., Rahimi G., Ghannad M., 2009, Set of field equations for thick shell of revolution made of functionally graded materials in curvilinear coordinate system, *Mechanics* **77**(3): 18-26.
- [11] Jabbari M., Nejad M.Z. , Ghannad M., 2015, Thermo-elastic analysis of axially functionally graded rotating thick cylindrical pressure vessels with variable thickness under mechanical loading, *International Journal of Engineering Science* **96**: 1-18.
- [12] Gharibi M., Nejad M.Z., Hadi A., 2017, Elastic analysis of functionally graded rotating thick cylindrical pressure vessels with exponentially-varying properties using power series method of Frobenius, *Journal of Computational Applied Mechanics* **48**(1): 89-98.
- [13] Zamani Nejad M., Jabbari M., Hadi A., 2017, A review of functionally graded thick cylindrical and conical shells, *Journal of Computational Applied Mechanics* **48**(2): 357-370.
- [14] Dehghan M., Baradaran G.H., 2011, Buckling and free vibration analysis of thick rectangular plates resting on elastic foundation using mixed finite element and differential quadrature method, *Applied Mathematics and Computation* **218**(6): 2772-2784.
- [15] Lin J.-Y., Chen H.-T., 1992, Radial axisymmetric transient heat conduction in composite hollow cylinders with variable thermal conductivity, *Engineering Analysis with Boundary Elements* **10**(1): 27-33.
- [16] Ebrahimi M., Vakilipour S., Shahverdi M., 2017, A novel computational procedure based on league championship algorithm for solving an inverse heat conduction problem, *Journal of Computational Applied Mechanics* **48**(2): 285-296.
- [17] Ozkan G., Mengi Y., 1997, On the use of FFT algorithm for the circumferential coordinate in boundary element formulation of axisymmetric problems, *International Journal for Numerical Methods in Engineering* **40**(13): 2385-2412.
- [18] Liu T.-W., Xu H.-H., Qiu X.-L., 2012, A combination method of mixed multiscale finite-element and laplace transform for flow in a dual-permeability system, *International Scholarly Research Notices* **2012**: 202893.
- [19] Noor A.K., Peters J.M., 1988, Stress and vibration analyses of anisotropic shells of revolution, *International Journal for Numerical Methods in Engineering* **26**(5): 1145-1167.
- [20] Sheinman I. , Weissman S., 1987, Coupling between symmetric and antisymmetric modes in shells of revolution, *Journal of Composite Materials* **21**(11): 988-1007.
- [21] Sivadas K., Ganesan N., 1992, Effect of coupling between symmetric and antisymmetric modes in composite thick shells of revolution, *Finite Elements in Analysis and Design* **11**(1):9-18.
- [22] Correia I.P., Barbosa J., Soares C.M.M., Soares C.A.M., 2000, A finite element semi-analytical model for laminated axisymmetric shells: statics, dynamics and buckling, *Computers & Structures* **76**(1-3): 299-317.
- [23] H. Santos, C. M. M. Soares, C. A. M. Soares , J. Reddy, A semi-analytical finite element model for the analysis of laminated 3D axisymmetric shells: bending, free vibration and buckling, *Composite Structures* **71**(3): 273-281.
- [24] Santos H., Soares C.M.M., Soares C.A.M., Reddy J., 2006, A finite element model for the analysis of 3D axisymmetric laminated shells with piezoelectric sensors and actuators, *Composite Structures* **75**(1): 170-178.
- [25] Santos H., Soares C.M.M., Soares C.A.M., Reddy J., 2008, A finite element model for the analysis of 3D axisymmetric laminated shells with piezoelectric sensors and actuators: bending and free vibrations, *Computers & Structures* **86**(9): 940-947.
- [26] Santos H., Soares C.M.M., Soares C.A.M., Reddy J., 2009, A semi-analytical finite element model for the analysis of cylindrical shells made of functionally graded materials, *Composite Structures* **91**(4): 427-432.
- [27] Heinrich B., 1996, The Fourier-finite-element method for Poisson's equation in axisymmetric domains with edges, *SIAM Journal on Numerical Analysis* **33**(5): 1885-1911.
- [28] Kim Y.P., Kweon J.R., 2009, The Fourier-finite element method for the Poisson problem on a non-convex polyhedral cylinder, *Journal of Computational and Applied Mathematics* **233**(4): 951-968.
- [29] Bakr S.A., Pardo D., Mannseth T., 2013, Domain decomposition Fourier finite element method for the simulation of 3D marine CSEM measurements, *Journal of Computational Physics* **255**: 456-470.
- [30] Lai J., Booker J.R., 1991, Application of discrete Fourier series to the finite element stress analysis of axi-symmetric solids, *International Journal for Numerical Methods in Engineering* **31**(4): 619-647.
- [31] Cho C., Ahn S., 2002, Transient thermoelastic analysis of disk brake using the fast Fourier transform and finite element method, *Journal of Thermal Stresses* **25**(3): 215-243.

- [32] Floquet A., Dubourg M., 1994, Nonaxisymmetric effects for three-dimensional analysis of a brake, *Journal of Tribology* **116**(3): 401-407.
- [33] Floquet A., Dubourg M., 1996, Realistic braking operation simulation of ventilated disk brakes, *Journal of Tribology* **118**(3): 466-472.
- [34] Jin G., Ma X., Shi S., Ye T., Liu Z., 2014, A modified Fourier series solution for vibration analysis of truncated conical shells with general boundary conditions, *Applied Acoustics* **85**: 82-96.
- [35] Jin G., Ye T., Jia X., Gao S., 2014, A general Fourier solution for the vibration analysis of composite laminated structure elements of revolution with general elastic restraints, *Composite Structures* **109**: 150-168.
- [36] Mohazzab A.H., Dozio L., 2015, Prediction of natural frequencies of laminated curved panels using refined 2-D theories in the spectral collocation method, *Curved Layer Structures* **2**: 1-14.
- [37] Mohazzab A.H., Dozio L., 2015, A spectral collocation solution for in-plane eigenvalue analysis of skew plates, *International Journal of Mechanical Sciences* **94**: 199-210.
- [38] Xie X., Zheng H., Jin G., 2015, Integrated orthogonal polynomials based spectral collocation method for vibration analysis of coupled laminated shell structures, *International Journal of Mechanical Sciences* **98**: 132-143.
- [39] Trefethen L.N., 2000, *Spectral Methods in MATLAB*, Siam.
- [40] Hetnarski R.B., Eslami M.R., Gladwell G., *Thermal Stresses: Advanced Theory and Applications*, Springer.